*Research Note*

# The Effect of Reservoir Length on Dam-Reservoir Interaction Analysis Based on the Compressible Fluid Assumption

**Amir Hooshang Akhaveissy[1]\* and Mohammad Malekshahi[2]**

1. Assistant Professor, Department of Civil Engineering, Razi University, Kermanshah, Iran,
* Corresponding Author; email: Ahakhaveissy@razi.ac.ir
2. M.Sc. Student, Department of Civil Engineering, Razi University, Kermanshah, Iran

## ABSTRACT

*In this study, the position of the truncation boundary, which is an important issue when modeling the reservoir in the finite element formulation and determining the hydrodynamic pressure on the dam, is investigated. Water in the reservoir is assumed to be compressible, and the Sommerfeld boundary is used to model the far field. The Euler-Lagrange method is used to analyze the reservoir-dam interaction. The serendipity element is used to model the reservoir and dam. The foundation is considered to be rigid. Most researchers assume that the truncation boundary is located three times the total height of the dam away from the dam body, and they use the Sommerfeld boundary at this location. For this purpose, the reservoir was disconnected at different intervals. The Pine Flat Dam is commonly analyzed with a Taft earthquake. The results of the analyses for different positions of the truncation boundary in reservoir models show that the position of the Sommerfeld boundary at five times the height of the dam away from the dam body is a proper place for the truncation boundary. Moreover, comparing the results of the present study based on the compressibility of water and those of previous research based on the incompressibility assumption indicates that the maximum hydrodynamic pressure is approximately 153.8% for a Taft earthquake. Therefore, the assumption of water compressibility plays an important role when evaluating the Pine Flat Dam.*

## 1. Introduction

In the study of fluid-structure interaction, one of the main problems is identifying the hydrodynamic pressure applied to the dam body during an earthquake. This issue plays a vital role in the safety evaluation of power generator nuclear reactors and many other industrial infrastructures; thus, fluid-structure interaction is a vast and unique subject that embraces all aspects of solid and fluid mechanics.

Analyzing a dam-reservoir system is much more complicated than analyzing the structure alone because of the difference between the characteristics of the fluid and the concrete on one side of the dam and the interaction between the reservoir and the dam on the other side.

In the 1970s, due to some damages occurred in a number of big dams, the dam interaction analysis was attracted in many researchers to work on the topic. One of the early methods is based upon fluid incompressibility assumption. Based on this assumption, Westergard solved the equation governing the hydrodynamic pressure in the dam reservoir domain (Helmholtz's equation) [1]. In this method for the

analysis of concrete dams, fluid is treated as an added mass to the body of the dam.

Then, the studies of Chopra [2-3] showed that the fluid incompressibility assumption does not predict correctly the applied hydrodynamic pressure on the dam body. Therefore, the earthquake engineering group in concrete dams has considered fluid compressibility in most concrete dams as an important factor in determining the earthquake response [4].

Previous studies on two-dimensional gravity dams root back to late 1970s, in which interaction effects were considered through the exact and non-numerical solutions of the governing equations [5-6].

Humar and Roufaiel [7] proposed a finite element model for the analysis and computation of hydro-dynamic pressure in an infinite reservoir of a gravity dam. They proposed an applicable boundary condition for a special seismic excitation frequency range. Sharan [8] proposed an effective method for the analysis of applied pressure on dams. This method is based on the finite element method in the frequency domain. Dissipation of energy was simulated by modeling of reservoir length as an infinite length and reservoir bottom sediments.

Ghaemian and Ghobarah [9] used staggered method in the problem of fluid-structure interaction. Hence, the staggered displacement method and the staggered pressure method were proposed to solve the fluid-structure interaction. Both of the methods are suitable for nonlinear analysis. Results expressed that even for large time steps; the displacement method provides more stable solutions. Previous studies assumed small displacement behavior for the fluid and also neglected the terms of transmission acceleration in the Navier-Stokes equation. However, Chen [10] studied the effects of surface flows and the nonlinearity of convective acceleration on the analysis of 2D gravity dams and reservoirs. In this study, not only nonlinear hydrodynamic pressures and the rise of the water surface but also the structural dynamic responses of the dam have been calculated. Comparison between the results of analyses with and without water surface effects showed that the surface wave effects of the fluid can be neglected in the dynamic structural analysis of a concrete gravity dam. Zienkiewicz and Taylor [11] explained the governing fluid-structure equations using the finite element method. For modeling the upstream boundary of the reservoir, they used radiative boundaries. Seghir et al. [12] used the coupled finite element and symmetric boundary element to model the interaction problem. In this study, fluid was assumed as incompressible and the location of the truncation boundary is considered at distances $L_F = 3 \times H_B$ and $L_F = 0.25 \times H_B$. That $L_F$ is the length of the reservoir and $H_B$ is the height of dam. Predicted hydrodynamic pressure by finite element method for the length of the reservoir equal to $0.25 \times H_B$ shows large values in comparison with boundary element method. However, the results of finite element method for the length of the reservoir equal to $3 H_B$ are in accordance with the results of the boundary element method.

Akkose et al. [13-14] analyzed the fluid-structure interaction for an arch dam. Three-dimensional eight-node elements with the Lagrange-Lagrange approach were used for the nonlinear analysis of the arch dam. The nonlinear behavior of the concrete dam was modeled by the Drucker-Prager criterion. Du et al. [15] studied the nonlinear seismic response of a foundation-arch dam system. The responses were determined based on the combination of the implicit finite element method, the transmitting boundaries and the "Relaxation" dynamic method. Comparison of responses between the proposed method and the common method of the analysis shows that the maximum dynamic stress from proposed method is lower than that of the common method. Aznarez et al. [16] analyzed the fluid-structure interaction with the effects of reservoir bottom absorbent materials. The boundary element method was applied for the analyses in the frequency domain. The effects of absorbent materials, degree of consolidation, compressibility and permeability were considered on the dynamic responses of the system. The nonlinear finite element method and boundary element method were respectively used to model the structure and fluid in the analysis of fluid-structure interaction problems in the time domain [17]. Maity and Bhattacharyya [18] studied different parameters on fluid-structure interaction problem. The parameters included the thickness of dam, modulus of elasticity and reservoir water level.

Mitra and Sinhamahapatra [19] used the finite element method to simulate the sloshing effect on a

water storage tank. Results of the analyses illustrated the hydro-dynamic pressure on flexible walls is more than the rigid walls. Bonnet et al. [20] used a combination of the finite element and boundary element methods to simulate the dam-reservoir interaction in the frequency domain. The analyses were implemented based on elastic behavior of material and a rigid reservoir bottom. The results of the analyses show good agreement between theoretical and numerical predictions.

Gogoi and Maity [21] analyzed the fluid-structure interaction in the frequency domain. The analyses were included the sloshing effects. The material behavior was assumed as linear-elastic and fluid as compressible. The Sommerfeld boundaries were used at distance $3H_B$ of the dam, $H_B$ is the height of the dam. Akkose et al. [22] focused on non-linear seismic response of a concrete gravity dam subjected to near-fault and far-fault ground motions including dam-water-sediment-foundation rock interaction. The results showed that the crest displacement values for near-fault ground motion are greater than those for far-fault ground motion, although the peak ground acceleration of near-fault and far-fault records are the same. According to presented results, it is apparent that the linear and non-linear seismic response of the gravity dam under near-fault ground motion is affected greater than those subjected to far-fault ground motion.

Wang et al. [23] proposed a procedure for the time-domain analysis of gravity dam-reservoir inter-action. In this procedure, the dam and a part of the reservoir with irregular geometry were modeled with finite elements. A high-order doubly asymptotic open boundary condition was developed to model the remaining part of the reservoir simplified as a semi-infinite layer of constant depth. In this paper, the same isoparametric finite elements were used in modeling the near field and the far field of a semi-infinite reservoir, and the open boundary condition is split into the Sommerfeld radiation boundary and an external nodal load. Numerical examples demonstrate the excellent performance of this present technique not only for early-time but also for long-time computations. Bayraktar et al. [24] investigated the effects of finite element (FE) model updating on nonlinear seismic response of arch dam-reservoir-foundation systems. In the analytical modeling, arch dam-reservoir-foundation interaction

was represented by Lagrangian approach. The results of this paper shows that, after model updating by adjusting material properties, the differences between initial analytical and experimental natural frequencies of Berke Dam are reduced. The displacements and the maximum principal stresses from an updated $F_E$ model are smaller than those of the initial $F_E$ model. The frequency content of the displacements, strains, and stresses obtained from an updated FE model are different from the initial model. Birk et al. [25] solved the dam-reservoir interaction problem, directly in the time-domain by modeling a part of the reservoir as a semi-infinite fluid-channel. Radiation damping is taken into account rigorously using an analytical solution with respect to the direction of wave propagation. The results showed that the accuracy of the model in the frequency-domain is governed by the refinement of the semi-discretization rather than the degree of rational approximation. In order to increase the applicability of the method, a description of the semi-infinite fluid region using polar coordinates, or more general scaled boundary coordinates, is desirable. Bouaanani and Lu [26] assessed the use of a potential-based fluid finite element formulation to investigate earthquake excited dam-reservoir systems. The results mainly illustrate that the potential-based formulation coupled with the boundary conditions discussed in the paper and enhanced post-processing capabilities can be advantageously and efficiently used to assess dam-reservoir seismic response.

Most engineers consider the fluid domain to be an infinite region; however, the reservoir has to be cut at a proper distance from the dam body by employing a truncation boundary condition like the Sommerfeld boundary. This type of boundary attracts the energy of waves to simulate propagation of waves to the far field. It should be noted that the appropriate location of the truncation boundary when using the Sommerfeld boundary has not been studied. Thus, in the present paper, the proper location for using truncation boundary condition is investigated assuming that the fluid is compressible. Then, the predicted results are compared with the predicted results by Seghir et al. [12], which were based on the incompressibility assumption.

For this purpose, a program was written in the FORTRAN language, and the eight-node

serendipity element with plane strain behavior is used to model the dam and reservoir. The Euler-Lagrange method is applied in finite element procedure to determine the hydrodynamic pressure in the fluid.

## 2. Governing Equation of Wave Propagation Through Fluid

Akkose et al. [13] provided a vast study on different references related to the problem of fluid-structure interaction in which the finite element method is used. According to this study, three methods ar used in solving the fluid-structure interaction problem through the use of the finite element method. These methods are: Westergard, Euler-Lagrange and Lagrange-Lagrange.

In the Westergard method; the effect of the reservoir is applied to the structure as an added mass. In this method, the effect of pseudo fluid stiffness matrix and the interaction between dam and reservoir is neglected during earthquake acting.

In the Lagrange-Lagrange method, the response of both structure and fluid is the displacement, and the governing equations of the dam and reservoir system are symmetric.

In the Euler-Lagrange method; displacement is assumed as the variable response of the structure, and the pressure or velocity potential function is assumed to be the variable response of the fluid. In this case, the coupled system equations are non-symmetric.

In this study, the Euler-Lagrange method is used to analyze the dam-reservoir interaction problem.

In both Eulerian and Lagrangeian methods, the governing equation of fluid-structure system is determined using wave propagation through the fluid by assuming linear compressibility and inviscosity. The wave propagation equation through fluid is as follows [11]:

$$\nabla^2_p = \frac{1}{c^2} \frac{\partial^2 p}{\partial t^2} = \frac{\rho}{k} \frac{\partial^2 p}{\partial t^2} \tag{1}$$

where $p$ is the pressure function and $c$ is the acoustic wave speed. If the fluid would be assumed as incompressible, Eq. (1) would take the following form [11]:

$$\nabla^2_p = 0 \tag{2}$$

This equation has been solved and studied by many researchers through different analytical and numerical methods. However, in this study, Eq. (1) is used to solve the fluid-structure interaction. Therefore, the boundary conditions of the governing equation as shown in Figure (1) are stated as below:
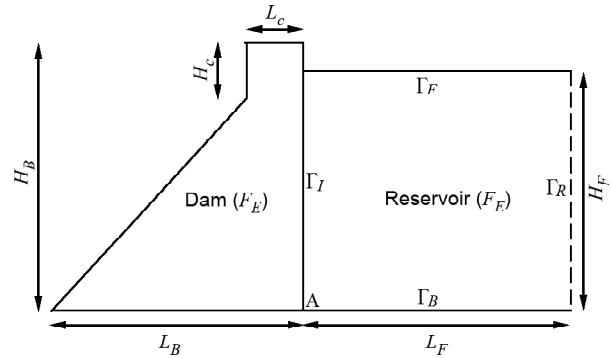


**Figure 1.** Dam-reservoir coupled model.

### 2.1. Reservoir Upstream Boundary ($G_R$)

Through the vibration of dam, volumetric waves due to hydrodynamic pressure are created in the reservoir. These waves would propagate toward the upstream. In cases that the length of the reservoir is infinity, these waves would finally vanish. In numerical modeling, it is common that the length of the reservoir would be a finite length. Therefore, in this case, a Sommerfeld-type radiation boundary condition is applied as:

$$\frac{\partial p}{\partial n} = -\frac{1}{c} \frac{\partial p}{\partial t} \tag{3}$$

### 2.2. Reservoir Bottom Boundary ($G_B$)

According to the rigidity of the reservoir bottom and assuming the earth moves horizontally, the pressure gradient is neglected for the $G_B$ boundary.

$$\frac{\partial p}{\partial n} = 0 \tag{4}$$

### 2.3. Reservoir Free Surface Boundary ($G_F$)

By neglecting the effects of surface waves, the governing boundary condition is as follows:

$$p = 0 \tag{5}$$

### 2.4. Fluid-Structure Interface ($G_I$):

The body of the dam is deformed during an

earthquake due to the inertia forces. The deformation is caused by hydrodynamic pressure in the reservoir which depends on compressibility assumptions. Then, the hydrodynamic pressure interacts with the body face of the dam ($G_I$). Consequently, the applied pressure on the dam caused by the inertia forces is as follows:

$$\frac{\partial p}{\partial n} = -\rho \times \ddot{u}_n \qquad (6)$$

where $\rho$ is the density of fluid, and $\ddot{u}_n$ is the structure's acceleration vector in the direction normal to the common boundary of the fluid and structure.

Using the Galerkin method, Eq. (1) can be rewritten as follows:

$$\int_{V_e} N_P^T \left[ \frac{1}{c^2} \frac{\partial^2 p}{\partial t^2} - \left( \frac{\partial^2 p}{\partial x^2} + \frac{\partial^2 p}{\partial y^2} \right) \right] dv = 0 \qquad (7)$$

where $N_P$, is the hydrodynamic nodal interpolation function in the finite element method. As a result, by using discretization in finite element method, and placement the boundary conditions in Eq. (7), the equation governing the fluid can be compacted as follows:

$$S\ddot{p} + \tilde{C}\dot{p} + Hp + Q^T\ddot{u} + q = 0$$

$$[S] = \int_{v_e} N_P^T \times \frac{1}{c^2} \times N_p \times d_v$$

$$[\tilde{C}] = \int_{G_R} N_P^T \times \frac{1}{c} \times N_p \times dG$$

$$[H] = \int_{v_e} (\nabla N_p)^T \times (\nabla N_p) \times dv \qquad (8)$$

$$q = \rho \times Q^T \times I \times \ddot{u}_{g(t)}$$

where $[S]$, $[\tilde{C}]$ and $[H]$ are pseudo mass matrix, pseudo damping matrix and pseudo fluid stiffness matrix, respectively.

## 3. Structure Governing Equations

Based on the theory of the finite element method [11], the governing equation of the dynamic response of the structure to support excitation in the time domain can be described as follows:

$$M\ddot{u} + C\dot{u} + Ku - Qp + M \times I \times \ddot{u}_g(t) = 0 \qquad (9)$$

where $[M]$, $[C]$ and $[K]$ are mass, damping and stiffness matrices of the structure, respectively. $u$, $\dot{u}$ and $\ddot{u}$ are displacement, velocity and acceleration vectors, respectively. In Eq. (9), $I$ is a unit matrix that

transforms the support acceleration vector $\{\ddot{u}_g(t)\}$ to the structure degrees of freedom. The role of matrix $Q$ is to transform the acceleration of the structure to pressure flux, and to transform the hydrodynamic pressure into applied loads on the structure. In fact, matrix $Q$ causes the interaction between fluid and structure. In the same relation, vector $\vec{n}$ is normal to the common surface of the structure and fluid. Hence, the coupled equation of the fluid-structure system based on relations (8) and (9) in the Euler-Lagrange formulation are presented as follows:

$$\begin{bmatrix} M & O \\ \rho Q^T & S \end{bmatrix} \begin{Bmatrix} \ddot{u} \\ \ddot{p} \end{Bmatrix} + \begin{bmatrix} C & 0 \\ 0 & \tilde{C} \end{bmatrix} \begin{Bmatrix} \dot{u} \\ \dot{p} \end{Bmatrix} +$$
$$\begin{bmatrix} K - Q \\ 0 & H \end{bmatrix} \begin{Bmatrix} u \\ p \end{Bmatrix} = \begin{bmatrix} -M \times I \times \ddot{u}_g(t) \\ -\rho Q^T \times I \times \ddot{u}_g(t) \end{bmatrix} \qquad (10)$$

A computer program is written in the FORTRAN language based on Eq. (10). The Pine Flat Dam is analyzed using the equations and the Sommerfeld boundary condition. Then, the results of the present work based on the compressible fluid assumption and using the Sommerfeld boundary conditions are compared with results of the analysis by Seghir et al. [11], which were based on the coupled finite element and symmetric boundary element method and on the incompressible fluid assumption. Finally, the response of Pine Flat Dam is evaluated with different boundary distances to determine an appropriate truncation boundary location.

## 4. Analysis of the Pine Flat Dam During the Taft Earthquake

Dynamic analysis of Pine Flat Dam is used to study the effect of fluid compressibility. The geometric properties and dimensions of the Pine Flat Dam are presented in Figure (1) and Table (1). The recorded horizontal component of the ground acceleration during the Taft earthquake (S69E) shown in Figure (2) is used in the analysis. Table (2) summarizes the

**Table 1.** Geometry and material properties of the Pine Flat Dam.

| Dimensions (m) | | | | | | Material Properties | | |
|---|---|---|---|---|---|---|---|---|
| $H_B$ | $H_C$ | $L_B$ | $L_C$ | $L_F$ | $H_F$ | $E$ (N/m²) | $n$ | $r$ (Kg/m³) |
| 122.0 | 18.5 | 96.0 | 9.75 | 366.0 | 116.0 | $34.47 \times 10^9$ | 0.2 | 2440 |

results of the periods for the first five free vibration modes. Figure (3) shows mesh of the system. The results of the present work and the ANSYS software (for the un-damped system) are compared in Figures (4) and (5). The eight-noded element with plane strain behavior is used for both models. A
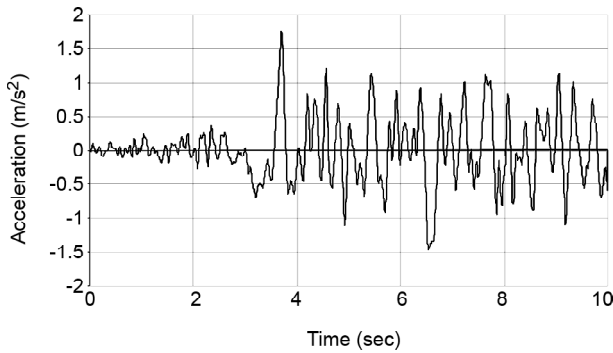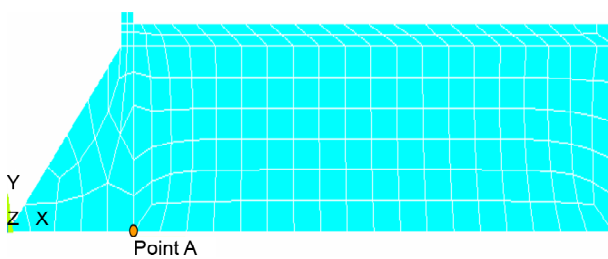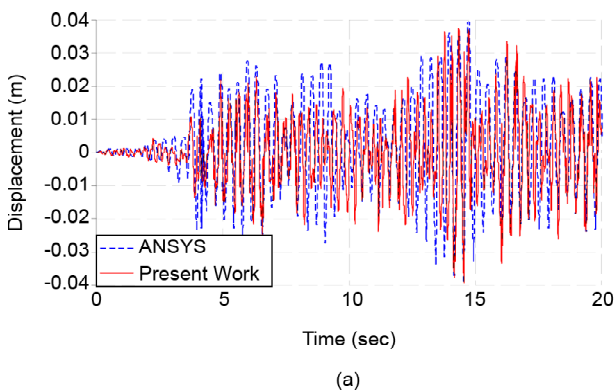
stiffness proportional damping equivalent to five percentage damping (5%) is used for all the modes. A time step of 0.005 sec is chosen for the analysis. The density and velocity of the pressure wave in fluid are set to 1000 and 1438.7, respectively. The dam and reservoir are discretized by the isoparametric eight-noded element with plane strain behavior.

The time history of horizontal displacement at the dam crest and the hydro dynamic pressure for present work are compared with predicted results by ANSYS software in Figure (4), respectively. Figure (5) shows comparison of predicted hydrodynamic pressure distribution from present work and ANSYS software when the hydrodynamic pressure at point A in Figure (3) is the maximum value. The comparisons in Figures (4) and (5) show good agreement between predicted results by present work and ANSYS software. However, Figures (4) and (5) show little differences between the results of present work and ANSYS software. The differences are due to the type of applied elements for both modeling. The four-noded element with the bi-linear
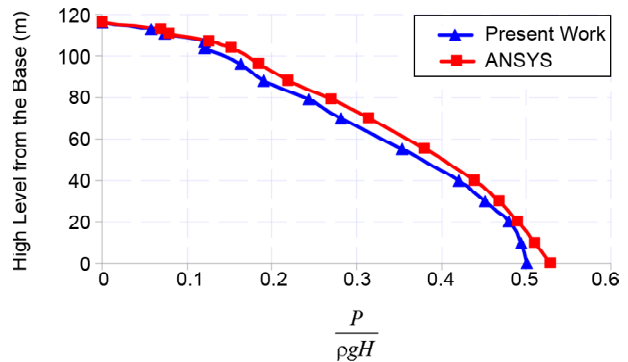


**Figure 2.** Horizontal ground acceleration record of the Taft earthquake.

**Table 2.** Geometry and material properties of the Pine Flat Dam.

| Mode Number | 1 | 2 | 3 | 4 | 5 |
|---|---|---|---|---|---|
| Dam Alone FE | 0.2558 | 0.1241 | 0.0921 | 0.0705 | 0.0466 |



**Figure 3.** Mesh of the dam and reservoir.



**Figure 5.** Hydrodynamic pressure distribution on upstream face of the dam under the Taft earthquake.
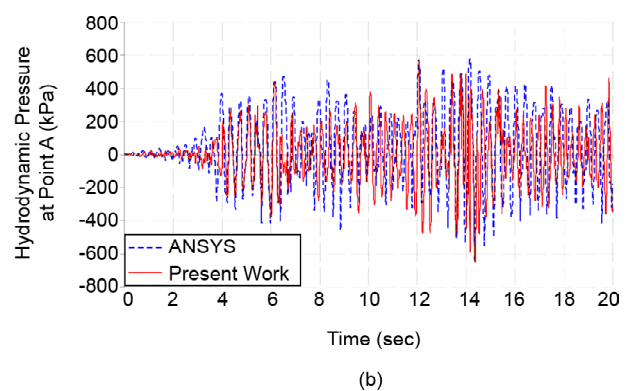


(a)



(b)

**Figure 4.** Time history analysis under the Taft earthquake 0.179g, a) Horizontal displacement of the dam crest, b) Hydrodynamic pressure of the dam heel.

shape function was used for modeling of the dam and fluid in ANSYS software, but the isoparametric eight-noded element, Serendipity element, with higher order shape function was used for modeling of the dam and fluid in present work. The predicted results from the proposed method are compared with the results of Seghir et al. [12] in Figure (6). It should be noted that the results shown [12] were obtained based on the fluid incompressibility assumption. This assumption causes the obtained hydrodynamic pressure to be lower than the real value. However, the results predicted in the present work are based on the compressible fluid assumption and use the Sommerfeld boundary condition.
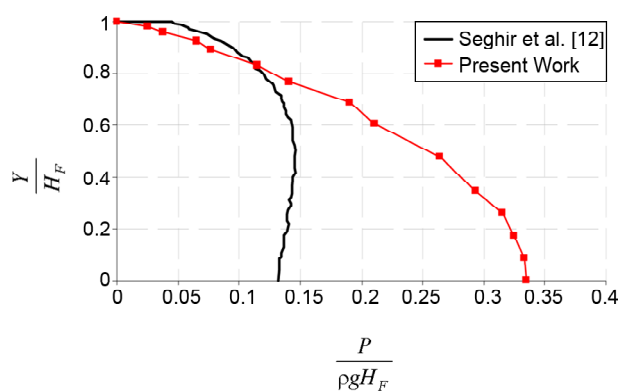


**Figure 6.** Hydrodynamic Pressure envelope acting on the upstream face of the dam.

In Figure (6), Y is the high level from the base. Figure (6) shows that the fluid compressibility assumption, present work, causes the hydrodynamic pressure to be greater than the predicted hydrodynamic pressure using the incompressible assumption by Seghir et al. [12]. Therefore, the incompressible fluid assumption causes a significant error in the evaluation of the hydrodynamic pressure applied to the dam body. Figure (6) shows that the maximum hydrodynamic pressures predicted from the compressibility and incompressibility assumptions are 380.7 kPa and 150 kPa, respectively. Hence, the results predicted using the compressible fluid assumption and the Sommerfeld boundary condition are more accurate than using the incompressible fluid assumption or the coupled finite element and symmetric boundary element method. Thus, the response of the Pine Flat Dam is studied for different near-field earthquakes to evaluate the frequency effects on the dam. The Taft, Elcentro, Chi-Chi and

Kobe earthquakes are selected as near-field earthquakes. The selected earthquakes are scaled to a maximum acceleration of 0.35 g, which is chosen such that the earthquake has a mean return period of 475 years and that a stronger earthquake will occur with a probability of 10%.
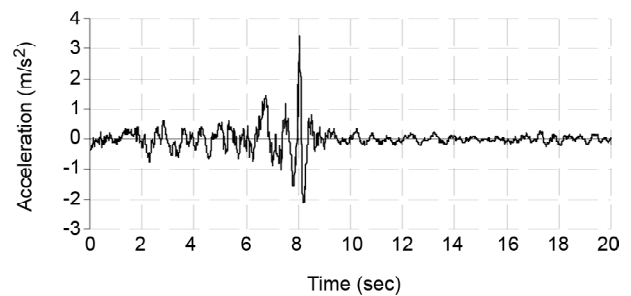
## 5. Frequency Analysis of Different Earthquakes

The Taft, Chi-Chi and Kobe earthquakes are applied to analyze the Pine Flat dam. These earthquakes are known as near-fault field. The recorded accelerations for different earthquakes are scaled to the peak ground acceleration 0.35g. Figure (7) shows scaled different earthquakes.
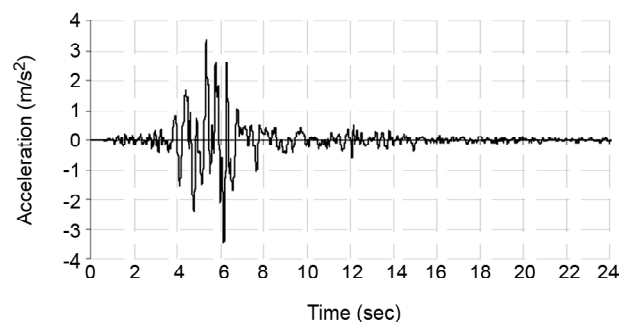
The contents of frequency of different earthquakes are evaluated to predict critical earthquake on Pine Flat dam. Therefore, the response of the dam-
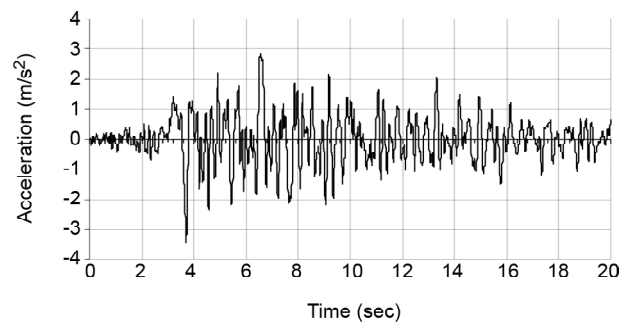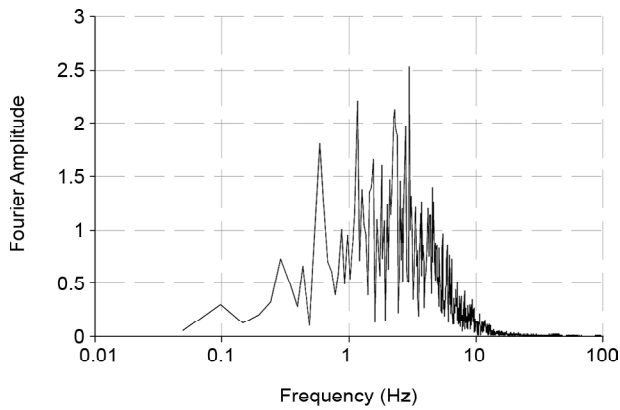


(a) Taft Earthquake, PGA = 0.35 g
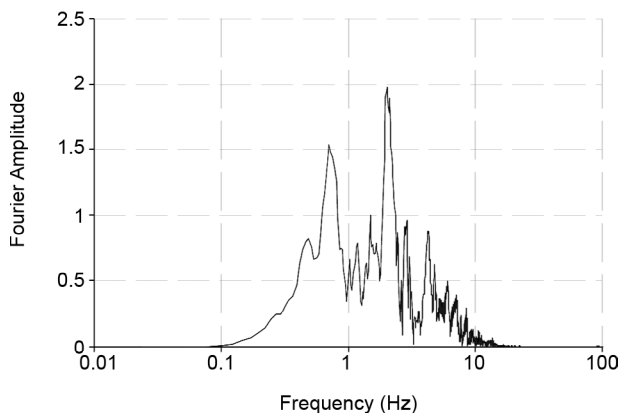


(b) Chi-Chi Earthquake, PGA = 0.35 g



(c) Kobe Earthquake, PGA = 0.35 g

**Figure 7.** Scaled recorded acceleration to 0.35g a), Taft b), Chi-Chi and c) Kobe earthquake.

reservoir system depends on contents of frequency of different earthquakes. Hence, the critical earthquake that causes the maximum hydrodynamic pressure on the dam body is determined by using the Fourier analysis. Then, after the analysis of the dam-reservoir system under different earthquakes, the validity of these analyses can be determined. The Fourier spectrum of Taft, Chi-Chi and Kobe earthquakes are shown in Figure (8) by using Fast Fourier Transform (FFT) analysis.



(a) Fourier Analysis for Taft Earthquake



(b) Fourier Analysis for Kobe Earthquake
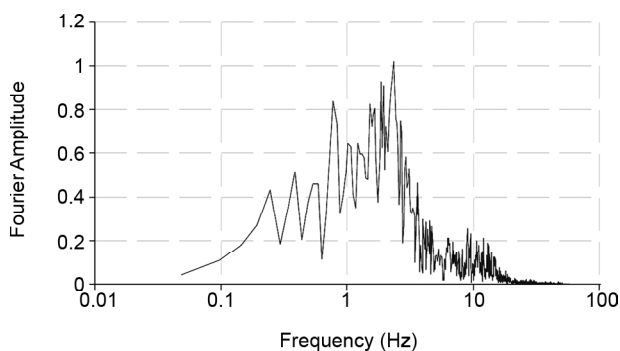


(c) Fourier Analysis for Chi-Chi Earthquake

**Figure 8.** Frequency analysis of scaled different earthquakes to 0.35g a) Taft, b) Kobe and c) Chi-Chi.

Extracted results from Figure (6) are shown in Table (3). $T_{max}$ in Table (3) shows the period in which determined Fourier amplitude of frequency analysis has the maximum value. Table (3) shows maximum Fourier amplitude is 2.527 for Taft earthquake, 1.981 for Kobe earthquake and 1.02 for Chi-Chi earthquake. Moreover, value of the Fourier amplitude at period first mode of the dam is 0.665 for Taft earthquake, 0.402 for Kobe earthquake and 0.0725 for Chi-Chi earthquake. Hence, the response of the dam is predicted to be a maximum value for Taft earthquake and then Kobe and Chi-Chi earthquakes, respectively.

**Table 3.** Summarized results of the frequency analysis for different earthquakes scaled to 0.35g.

| Earthquake | Taft | Kobe | Chi-Chi |
|---|---|---|---|
| P.G.A | 0.35g | 0.35g | 0.35g |
| $T_{max}$ (sec) | 0.3360 | 0.4930 | 0.4270 |
| Fourier amplitude at $T_{max}$ | 2.5270 | 1.9810 | 1.0200 |
| Period first mode only for the structure of the dam ($T_S$) | 0.2558 | 0.2558 | 0.2558 |
| Fourier Amplitude at $T_S$ | 0.6650 | 0.4020 | 0.0725 |

According to Fourier analysis, the Taft earthquake is the ruling earthquake. Thus the dynamic response of the dam-reservoir systems under the Taft earthquake is investigated.

Figure (9) shows the hydrodynamic pressure on the heel and the horizontal displacement of dam crest under the Taft earthquake. The analyses was performed both for the damped and undamped conditions.

## 6. Dynamic Analysis of the Pine Flat Dam with Different Reservoir Lengths

Previous investigations have shown that the position of the truncation boundary has a significant effect on the hydrodynamic pressure on the dam body; however, in the past, many studies have chosen the location of truncation boundary to be $3H_B$ from the dam body [12].

Moreover, it should be noted that when choosing the position of the truncation boundary in the upstream region model, the hydrodynamic pressure may not be calculated correctly. Thus, the distances of the location of the truncation boundary are selected as $3HB$, $5H_B$, $7H_B$, $10H_B$, $15H_B$, $23H_B$ and $50H_B$. The

analyses were performed both for the damped and undamped conditions. The first and fifth modes of the damped condition were used to determine the stiffness matrix coefficients. The results are presented for the heel of the dam (point A).

As observed from Table (4), the hydrodynamic pressure at the bottom of the upstream face of the dam (i.e., the dam heel) in both damped and undamped conditions has little variation when the boundary is beyond $5H_B$.

However, the values of the maximum hydrodynamic pressure on the dam body at $5H_B$ are considerably different than those for $3H_B$ both in

the damped and undamped conditions. The ratio of the maximum hydrodynamic pressure, when the reservoir length is $3H_B$ and the distance is $5H_B$ for the damped and undamped conditions are 1.260 and 1.768, respectively.

Figure (10) shows the distribution of the hydrodynamic pressure on the dam body under the damped and undamped conditions. The horizontal axis in this figure is normalized to the maximum hydrostatic pressure. The hydrodynamic pressure distribution for $3H_B$ is greater than that for the other distances. However, the hydrodynamic pressure distributions for reservoir lengths between $5H_B$ and $50H_B$ are
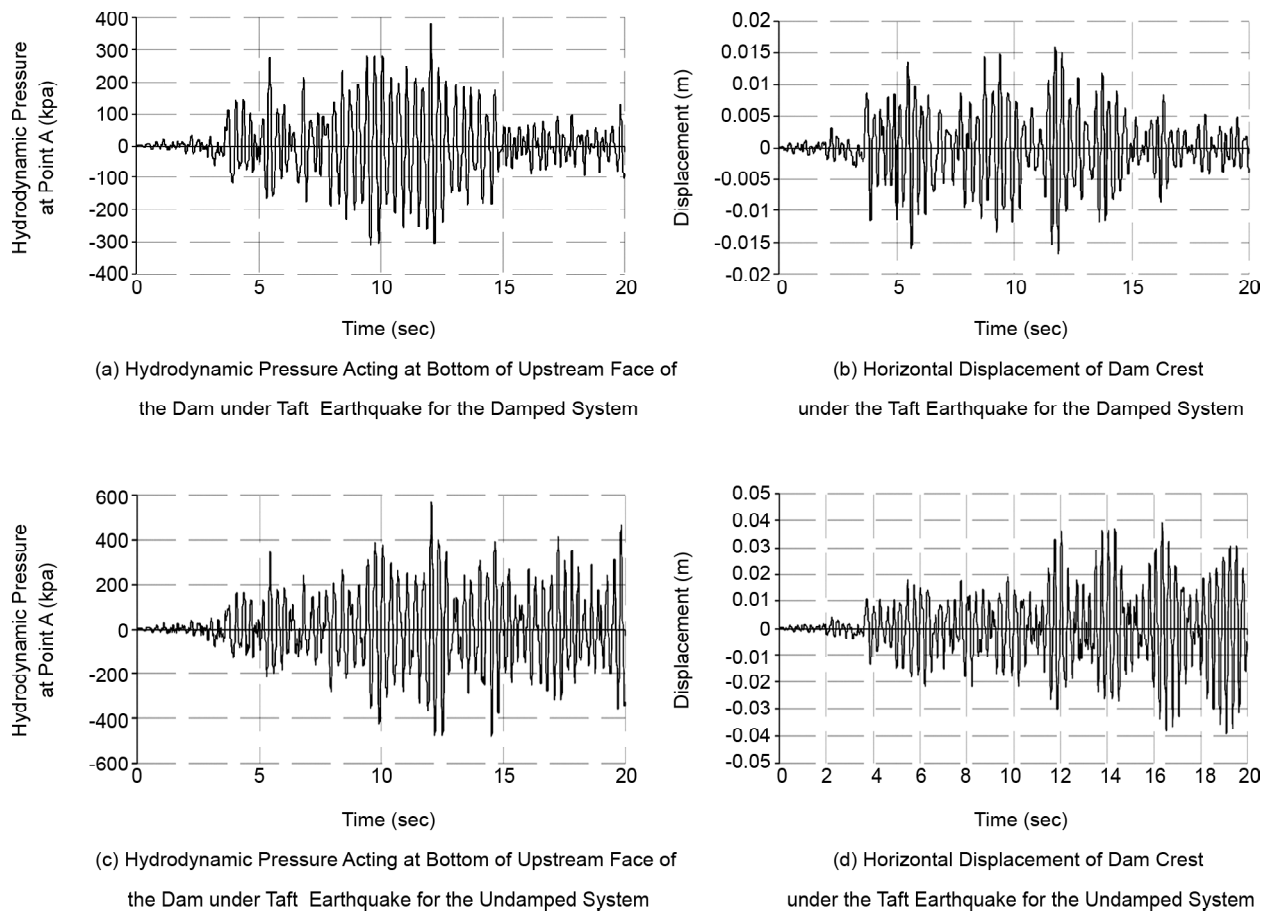


(a) Hydrodynamic Pressure Acting at Bottom of Upstream Face of the Dam under Taft Earthquake for the Damped System

(b) Horizontal Displacement of Dam Crest under the Taft Earthquake for the Damped System

(c) Hydrodynamic Pressure Acting at Bottom of Upstream Face of the Dam under Taft Earthquake for the Undamped System

(d) Horizontal Displacement of Dam Crest under the Taft Earthquake for the Undamped System

**Figure 9.** Analysis time history of hydrodynamic pressure at bottom of upstream face of the dam and analysis time history of horizontal displacement of dam crest under the Taft earthquake.

**Table 4.** Time history response of the hydrodynamic pressure acting at the bottom of the upstream face of the dam (point A).

| Length of Reservoir | $3H_B$ | $5H_B$ | $7H_B$ | $10H_B$ | $15H_B$ | $23H_B$ | $50H_B$ |
|---|---|---|---|---|---|---|---|
| **Damped** | | | | | | | |
| P (kPa) | 744.2 | 590.35 | 471.87 | 643.97 | 509.94 | 565.05 | 540 |
| **Undamped** | | | | | | | |
| P (kPa) | 1115.2 | 630.5 | 696.45 | 773 | 621.7 | 668 | 623.78 |

close together. Thus, a reservoir length of $5H_B$ is economic for numerical analyses. However, the results based on $5H_B$ are close to those based on $50H_B$, and the value of the hydrodynamic pressure for $5H_B$ is a little more than that for $50H_B$. Consequently, assuming a reservoir length of $5H_B$ is economic and can be used to analyze reliably the dam-reservoir interaction under earthquake excitation. The distribution of hydrodynamic pressure in the reservoir is shown in Figure (11) when the pressure of the heel point of dam is at its maximum value. Figure (11a) shows a region with zero pressure for undamped system while this phenomenon

is not occurred for damped system, Figure (11b). The region with zero pressure is occurred for both damped and undamped system when the length of reservoir is $15H_B$, Figure (12).

Comparison between results for the length of the reservoir equal to $5H_B$ and $15H_B$ shows that the negative pressure or cavitations' phenomenon is occurred at the end of the reservoir with the length of $15H_B$. Hence, the region with zero pressure and the negative pressure created chaos at the bottom of the reservoir. Consequently, a series of hillocks are created at bottom of the reservoir. These hillocks may cause larger hydrodynamic pressure on the
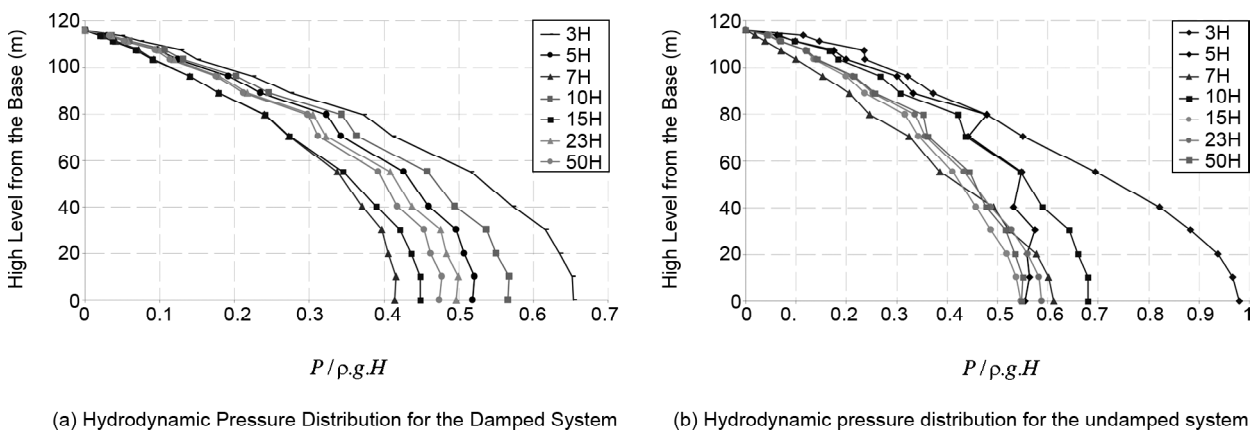


(a) Hydrodynamic Pressure Distribution for the Damped System

(b) Hydrodynamic pressure distribution for the undamped system

**Figure 10.** Hydrodynamic Pressure envelope acting on the upstream face of the dam with different reservoir lengths for the a) damped and b) undamped conditions.
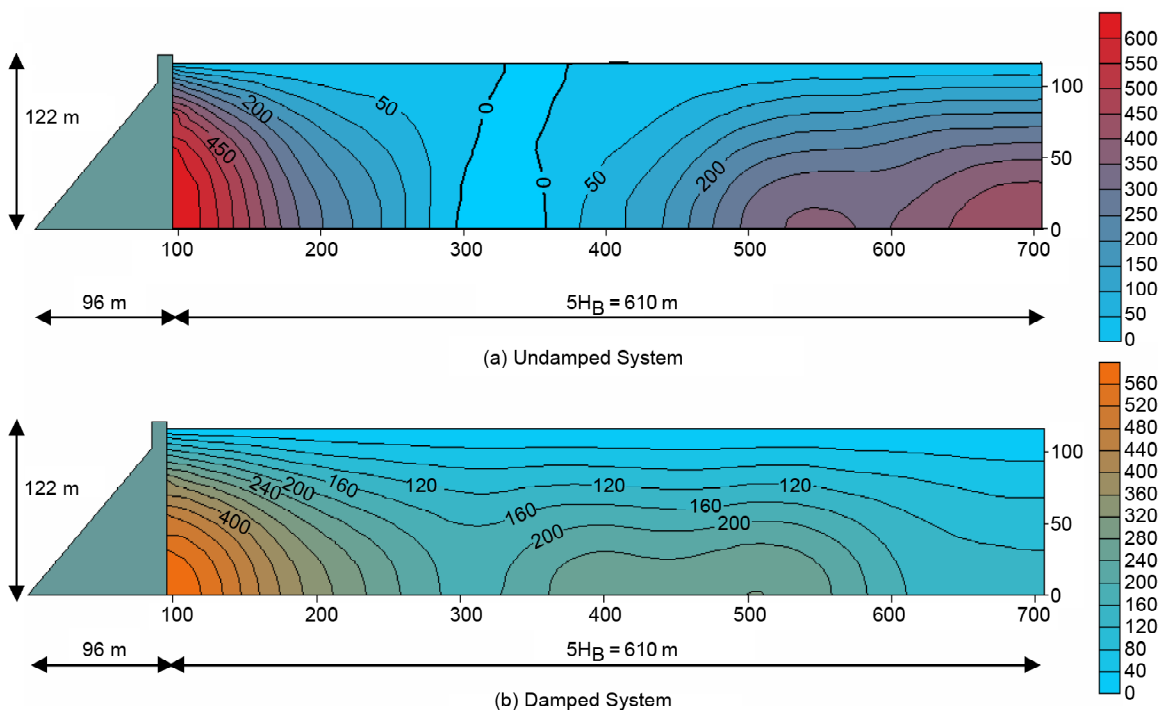


(a) Undamped System

(b) Damped System

**Figure 11.** Variation of the hydrodynamic pressure in the reservoir for the length equal to $5H_B$ when the pressure of the heel of the dam is at its maximum value.
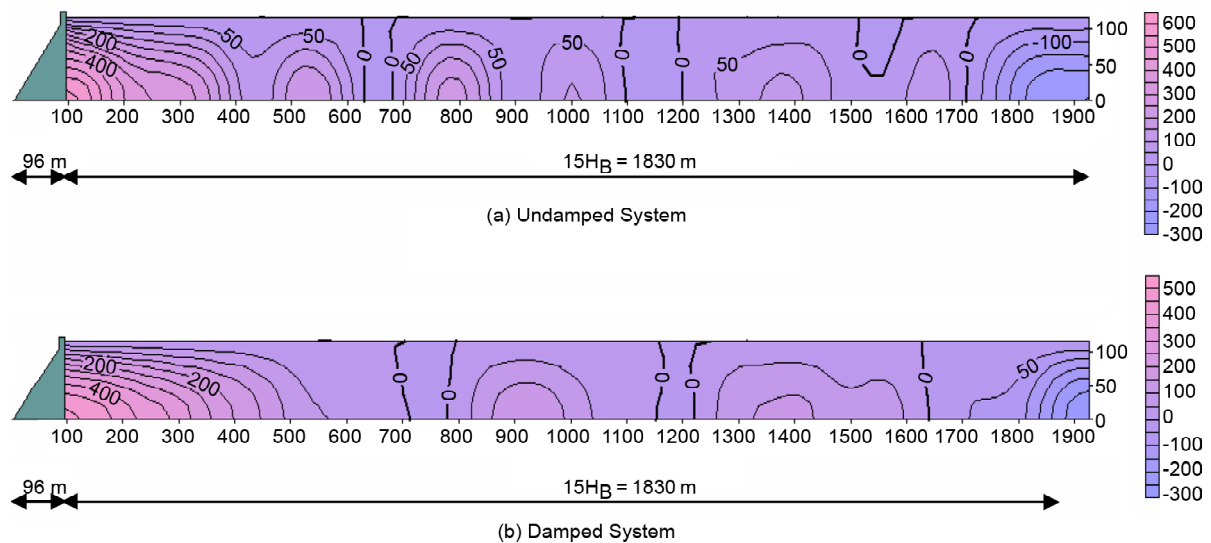
(a) Undamped System



(b) Damped System

**Figure 12.** Variation of the hydrodynamic pressure in the reservoir for the length equal to $15H_B$ when the pressure of the dam is at its maximum value.

dam than the pressures shown in Figure (12) when next similar earthquakes are occurred in presence of these hillocks.

## 6. Conclusion

In this study, the fluid compressibility effect was considered using dynamic analysis of the Pine Flat Dam in the Taft earthquake. For this purpose, a program was written in FORTRAN language in which an eight-node serendipity element with plane strain behavior was used to model the dam-reservoir system. In this study, the foundation was assumed to be rigid, and the fluid was assumed to be inviscous and compressible. The analysis determines the maximum applied hydrodynamic pressure on the dam body by assuming that the fluid compressibility is 2.5 times greater than that with the fluid incompressibility assumption. Then, the proper location for the truncation boundary condition was investigated to model the upstream region of the reservoir. For this purpose, the reservoir was cut at distances $3H_B$, $5H_B$, $7H_B$, $10H_B$, $15H_B$, $23H_B$ and $50H_B$, from the dam body. According to the performed analyses and Figure (10), for both damped and undamped conditions, the reservoir should be divided at $5H_B$ from the dam body in both damped and undamped conditions; beyond this distance, the distribution of hydrodynamic pressures is almost consistent, and as the reservoir length increases, the hydrodynamic pressure on the dam body does not change significantly. Due to the importance of the position of the truncation boundary in determining the hydrodynamic pressure on body dam, the horizontal length of the reservoir should be five times the total height of the dam to model the reservoir using the finite element method based on the results.

## References

1. Westergard, H.M. (1933) Water pressure on dams during earthquakes. *Transactions ASCE*, **98**, 418-472.

2. Chopra, A.K. (1967) Hydrodynamic pressure on dams during earthquakes. *Journal of Engineering Mechanics,* ASCE, **93**, 205-223.

3. Chopra, A.K. (1970) Earthquake response analysis of concrete gravity dams. *Journal of Engineering Mechanics,* ASCE, **96**(4), 443-454.

4. National Research Council, Earthquake Engineering for Concrete Dams: Design, Performance, and Research Needs, Washington, DC: The National Academies Press (1990).

5. Dasgupta, G. and Chopra, A.K. (1979) Dynamic stiffness matrices for homogeneous viscoelastic half plane. *Journal of Engineering Mechanics,* ASCE, **105**, 729-745.

6. Chopra, A.K. and Chakrabarti, P. (1981) Earthquake analysis of concrete gravity dams including dam-water-foundation rock interaction. *Earthquake Engineering and Structural*

*Dynamics*, **9**, 363-383.

7. Humar, J. and Roufaiel, M. (1983) Finite element analysis of reservoir vibration. *Journal of Engineering Mechanics,* ASCE*,* **109**(1), 215-231.

8. Sharan, S.K. (1992) Efficient finite element analysis of hydrodynamic pressure on dams. *Computers and Structures*, **142**(5), 713-723.

9. Ghaemian, M. and Ghobarah, A. (1998) Staggered solution schemes for dam-reservoir interaction. *Journal of Fluids and Structures*, **12**, 933-948.

10. Chen, B.F. (1996) Nonlinear hydrodynamic effects on concrete dam. *Engineering Structures*, **19**(3), 201-212.

11. Zienkiewicz, O.C. and Taylor, R.L. (2000) *The Finite Element Method*, Vol. 1: The basis, Fifth edition, Butterworth-Heinemann, Oxford.

12. Seghir, A., Tahakourt, A., and Bonnet, G. (2009) Coupling FEM and symmetric BEM for dynamic interaction of dam-reservoir systems. *Engineering Analysis with Boundary Elements*, **33**, 1201-1210.

13. Akkose, M., Adanur, S., Bayraktar, A., and Dumanoglu, A.A. (2008) Elasto-plastic earthquake response of arch dams including fluid-structure interaction by the lagrangian approach. *Applied Mathematical Modelling*, **32**, 2396-2412.

14. Akkose, M., Bayraktar, A., and Dumanoglu, A.A. (2008) Reservoir water level effects on nonlinear dynamic response of arch dams. *Journal of Fluids and Structures*, **24**, 418-435.

15. Du, X., Zhang, Y., and Zhang, B. (2007) Nonlinear seismic response analysis of arch dam-foundation systems- part I dam-foundation rock interaction. *Bulletin of Earthquake Engineering*, **5**, 105-119.

16. Aznarez, J.J., Maeso, O., and Dominguez, J. (2006) BE analysis of bottom sediments in dynamic fluid-structure interaction problems. *Engineering Analysis with Boundary Elements*, **30**, 124-136.

17. Czygan, O. and Estorff, O.V. (2002) Fluid-structure interaction by coupling BEM and nonlinear FEM. *Engineering Analysis with Boundary Elements*, **26**, 773-779.

18. Maity, D. and Bhattacharyya, S.K. (2003) A parametric study on fluid-structure interaction problems. *Journal of Sound and Vibration*, **263**, 917-935.

19. Mitra, S. and Sinhamahapatra, K.P. (2008) 2D simulation of fluid-structure interaction using finite element method. *Finite Elements in Analysis and Design*, **45**, 52-59.

20. Bonnet, G., Seghir, A., and Corfdir, A. (2009) Coupling BEM with FEM by a direct computation of the boundary stiffness matrix. *Computer Methods in Applied Mechanics and Engineering*, **198**, 2439-2445.

21. Gogoi, I. and Maity, D. (2010) A novel procedure for determination of hydrodynamic pressure along upstream face of dams due to earthquakes. *Computers and Structures*, **88**, 539-548.

22. Akkose, M. and Simsek, E. (2010) Non-Linear seismic response of concrete gravity dams to near-fault ground motions including dam-water-sediment-foundation interaction. *Applied Mathematical Modelling*, **34**, 3685-3700.

23. Wang, X., Jin, F., Prempramote, S., and Song, C. (2011) Time-domain analysis of gravity dam-reservoir interaction using high-order doubly asymptotic open boundary. *Computers and Structures*, **89**, 668-680.

24. Bayraktar, A., Sevim, B., and Altunisik, A.C. (2011) Finite element model updating effects on nonlinear seismic response of arch dam-reservoir-foundation systems. *Finite Elements in Analysis and Design*, **47**, 85-97.

25. Birk, C. and Ruge, P. (2007) Representation of radiation damping in a dam-reservoir interaction analysis based on a rational stiffness approximation. *Computers and Structure*s, **85**, 1152-1163.

26. Bouaanani, N. and Lu, F.Y. (2009) Assessment of potential-based fluid finite elements for seismic analysis of dam-reservoir systems. *Computers and Structures*, **87**, 206-224.